THE BELL SYSTEM
TECHNICAL JOURNAL

VOLUME XXXVIII MARCH 1959 NUMBER 2

The Three-Level Solid State Traveling-Wave Maser*

By R. W. DeGRASSE, E. O. SCHULZ-DuBOIS, and H. E. D. SCOVIL

(Manuscript received December 18, 1958)

Broadband very-low-noise microwave amplification can be obtained from solid state maser action in a propagating microwave structure. Such a traveling-wave maser produces unilateral amplification with a high degree of gain stability. The theory of the traveling-wave maser is developed and used to compare the gain, bandwidth and gain stability of the traveling-wave maser with that of the cavity maser. The general requirements for traveling-wave maser slow-wave structures are discussed. Theoretical analysis and experimental results are presented for the comb-in-waveguide slow-wave structure.

A traveling-wave maser consisting of a ruby-loaded comb structure was tested. A gain of 23 db at 6 kmc with a bandwidth of 25 mc was obtained. Further performance characteristics of this amplifier and one using gadolinium ethyl sulfate are given. Experimental verification of the low noise temperature of solid state masers was obtained.

I. INTRODUCTION

The three-level solid state maser, as proposed by Bloembergen,[1] employs a microwave pump signal to alter the thermal equilibrium of a

* This work was supported in part by the U. S. Army Signal Corps under Contract DA-36-039 sc-73224.

paramagnetic salt in such a manner that an otherwise absorptive medium becomes emissive when stimulated by radiation at the signal frequency. Successful application of this principle to produce microwave amplification was reported by Scovil *et al.*,[2,3] who used microwave cavities to couple the microwave radiation to the paramagnetic salt. Several laboratories[4,5] have since operated such cavity-type masers.

Microwave amplification can also be obtained by stimulating radiation from active material in a propagating structure. Effective coupling of the microwave fields to the paramagnetic salt is obtained by slowing the velocity of propagation of the microwave energy through the structure. The active material produces an equivalent negative resistance in the slow-wave structure, and a propagating wave having an exponentially increasing amplitude is obtained.

However, if a slow-wave structure is simply filled with the active material, the device will be reciprocal and have gain in both directions. It would therefore require excellent input and output matches and presumably external isolation to obtain unilateral gain. Unidirectional traveling-wave amplification can be obtained in a slow-wave structure which has definite regions of circular polarization of the magnetic field if a maser material is employed which has circularly polarized signal-frequency transitions. The maser material is then loaded in the structure in such a manner that it is coupled to the structure only for one direction of wave propagation. Then, the maser will have high gain in one direction and little or no gain in the reverse direction.

Unidirectional gain alone is not enough to ensure freedom from regenerative instability. One might add reciprocal loss, as in the case of the traveling-wave tube. However, the traveling-wave tube has an electron beam to carry the microwave energy past the loss region, with very little forward attenuation; in the case of the traveling-wave maser, only the one propagation wave is present and the attenuation subtracts directly from the forward gain. Unidirectional loss may be obtained in the same manner as the unidirectional gain, that is, by excitation of a magnetic material through a circularly polarized magnetic field. For the magnetic material, one may use either an absorptive ferrimagnetic material or an absorptive paramagnetic material whose thermal equilibrium is not disturbed by the microwave pump power.

II. TRAVELING-WAVE MASER THEORY

The amplification in a traveling-wave maser is obtained from power transferred to the microwave circuit by coherent excitation of the paramagnetic spins due to the magnetic fields of the circuit. This effect can

be represented classically in the constitutive equation of electromagnetic theory†

$$B = \mu_0(H + M_m), \tag{1}$$

where μ_0 is the permeability of free space and M_m is the magnetic moment per unit volume of maser material. The magnetic moment, M_m, is computed from the quantum mechanical treatment of the paramagnetic spin system. From this analysis may be obtained a complex permeability, given by

$$\chi' - j\chi'' = \frac{M_m}{H}. \tag{2}$$

The real part of the permeability, χ', will produce reactive effects in the microwave circuit, while the imaginary part can produce gain or loss. In most cases, the magnetic permeability depends upon the orientation of the magnetic field, H; thus, it is in general a tensor quantity.

If we have a microwave structure uniform in the z direction and partially filled with a maser material, the rate of change of power in the circuit with distance is given by

$$\frac{dP}{dz} = -\frac{1}{2}\omega\mu_0 \int_{A_m} H \cdot \chi'' \cdot H^* \, dS, \tag{3}$$

where the integration is performed over the cross section of the maser material, A_m. The power in the waveguide is given by

$$P = \frac{1}{2} v_g \mu_0 \int_{A_s} H^2 \, dS, \tag{4}$$

where v_g is the group velocity in the waveguide circuit, and the integration is performed over the entire waveguide cross section, A_s. The gain in a length of structure, l, is then given by

$$G = \frac{P(l)}{P(0)} = \exp\left[-\chi''_{\max} F(\omega/v_g) l\right], \tag{5}$$

where $\chi''_{\max}$ is the magnitude of the diagonalized χ'' tensor, and the filling factor, F, is defined by

$$F \equiv \frac{\int_{A_m} H \cdot \chi'' \cdot H^* \, dS}{\chi''_{\max} \int_{A_s} H^2 \, dS}. \tag{6}$$

† All equations are given in MKS units.

Rather than use the exact tensor representation for χ'', it is convenient to obtain a value for χ'' which reflects the magnetic field orientation. In a cavity maser, χ'' would be defined for linear polarization. In a traveling-wave maser, however, it is desirable to obtain nonreciprocal effects by using circularly polarized magnetic fields to excite the signal transition in the maser material.

In a maser material with small zero field splitting, such as gadolinium ethyl sulfate, the signal transitions have nearly pure circular polarization. Thus, if the magnetic fields of the circuit are resolved into circular polarized components, H_+ and H_-, the filling factor and gain (in decibels) are given by

$$F_+ = \frac{\int_{A_m} H_+^2 \, dS}{\int_{A_s} (H_+^2 + H_-^2) \, dS}, \tag{7}$$

$$G_{db} = -27.3\chi_+'' F_+ \frac{fl}{v_g}, \tag{8}$$

where f is the signal frequency.

The permeability for positive circular polarization, χ_+'', can be calculated using the notation of Schulz-DuBois.[6] He obtains for the rate of transition per ion from a state $\bar{n}$ to a state $\bar{n}'$,

$$w_{\bar{n}\to\bar{n}'}(S_+) = \frac{1}{2}\left(\frac{\pi g\beta}{h}\right)^2 g(f - f_0) \mid \langle \bar{n}' \mid S_+ \mid \bar{n} \rangle \mid^2 H_+^2, \tag{9}$$

where positive circular polarization is assumed as indicated by S_+. The power absorbed per unit volume of material is then

$$P = (\rho_{\bar{n}} - \rho_{\bar{n}'}) hf w_{\bar{n}\to\bar{n}'}(S_+), \tag{10}$$

where $\rho_{\bar{n}}$ is the density of ions in energy state $\bar{n}$ per unit volume.

The power absorbed per unit volume is given classically in terms of χ_+'' as

$$P = \tfrac{1}{2}\omega\mu_0\chi_+'' H_+^2. \tag{11}$$

Thus, χ_+'' is given by

$$\chi_+'' = \frac{\pi}{2\mu_0 h}(g\beta)^2(\rho_{\bar{n}} - \rho_{\bar{n}'}) g(f - f_0) \mid \langle \bar{n}' \mid S_+ \mid \bar{n} \rangle \mid^2. \tag{12}$$

If the equilibrium spin populations are inverted by making $\rho_{\bar{n}'}$ greater than $\rho_{\bar{n}}$, χ_+'' will be negative and amplification is obtained. The various conditions for maser population inversion have been discussed by Scovil.[3] A companion paper in this issue[7] discusses this problem in more detail.

For the case of propagation of energy in the reverse direction through the amplifier, the magnetic field sense of polarization will reverse and the filling factor will become

$$F_- = \frac{\int_{A_m} H_-^2 \, dS}{\int_{A_s} (H_+^2 + H_-^2) \, dS}. \tag{13}$$

The degree of nonreciprocity of gain is then determined by the ratio, R_m, given by

$$R_m = \frac{\int_{A_m} H_+^2 \, dS}{\int_{A_m} H_-^2 \, dS}. \tag{14}$$

This ratio must be optimized in the selection of a suitable slow-wave structure for use in the amplifier.

As was mentioned before, nonreciprocity in gain is not enough to insure that the amplifier will not have regenerative effects due to mismatched input and output terminations. Thus, it is necessary to also include some nonreciprocal loss for isolation. Both ferrimagnetic and paramagnetic isolators have been used. By increasing the concentration of the active ion in the maser crystal, it is possible to prevent maser action. Such a high-concentration crystal will have energy levels which are identical to the maser material; thus, it will provide nonreciprocal loss at the desired magnetic field and orientation. Ferrimagnetic isolators can be designed to operate at the magnetic field required by the maser material by using shape anisotropy to change the frequency of ferrimagnetic resonance.

The isolator loss is determined by (5). If we retain the convention that H_+ produces excitation of magnetic spins for propagation in the direction of amplification, and H_- for the reverse direction, then the isolator loss in the reverse direction is given by

$$L = 27.3 \chi''_{i+} F_{i-} \frac{fl}{v_g}, \tag{15}$$

where

$$F_{i-} = \frac{\int_{A_i} H_-^2 \, dS}{\int_{A_s} (H_-^2 + H_+^2) \, dS} \tag{16}$$

and χ''_{i+} is the lossy permeability of the isolator. The ratio of reverse loss to forward loss, R_i, then is the figure of merit of the isolator:

$$R_i = \frac{\int_{A_i} H_-{}^2\, dS}{\int_{A_i} H_+{}^2\, dS}. \tag{17}$$

In general, the figure of merit of a paramagnetic isolator will be about the same as that of the paramagnetic maser material. Since χ''_i is usually much greater for a ferrimagnetic than for a paramagnetic, it is possible to locate a ferrimagnetic isolator of small cross section in a region which will optimize R_i.

Some loss, L_0, will occur in the TWM structure due to the usual resistive losses in the conductors. This loss is reduced below the usual room temperature value by a factor of 2 to 4 by operation at liquid helium temperatures. In some cases this insertion loss can be quite high, and care must be exercised in the selection of a circuit. Uniform current distribution and the largest possible surface area in the circuit conductors are desirable.

In discussing TWM circuits, it is useful to rewrite the factor fl/v_g as the product of the slowing factor, S, and the number of free space wavelengths in the length of the structure, N, where

$$S = \frac{c}{v_g}, \qquad N = \frac{l}{c/f}. \tag{18}$$

Then the over-all maser forward gain and reverse loss equations are

$$G = 27.3SN\left(-\chi''_+F_+ - \chi''_{i+}\frac{F_{i-}}{R_i}\right) - L_0, \tag{19}$$

$$L = 27.3SN\left(\chi''_+\frac{F_+}{R_m} + \chi''_{i+}F_{i-}\right) + L_0. \tag{20}$$

For short-circuit stability of the amplifier, L must exceed G. In some cases, it may even be desirable to have L as much as 20 db greater than G, in order to eliminate any regenerative gain effects due to load changes. It is often convenient to refer to the product χ''_+F_+ as the inverse of the magnetic Q of the maser material. The magnetic Q will be defined for amplification in the forward direction as a positive number,

$$Q_m = \frac{-1}{\chi''_+F_+}. \tag{21}$$

Thus, the gain of the maser material only is simply

$$G = 27.3 \frac{SN}{Q_m} . \tag{22}$$

The frequency variation of the TWM gain is given primarily by the term $g(f - f_0)$ in (12). If a Lorentzian line shape is assumed for the maser material, then

$$g(f - f_0) = \frac{2}{\pi B_m} \frac{1}{1 + \left(2 \frac{f - f_0}{B_m}\right)^2} , \tag{23}$$

where B_m is the bandwidth over which χ'' is greater than one half its peak value. If we assume that the permeability is an analytic function, then it follows that, for the Lorentzian line shape,

$$\chi'_+ = -2 \frac{f - f_0}{B_m} \chi''_+ . \tag{24}$$

This rapid variation of χ'_+ in the vicinity of the amplifying region will produce some perturbation in the phase velocity characteristics of the slow-wave structure. However, in a broadband maser slow-wave structure this effect will be negligible. Using the frequency variation of (23), we obtain for the 3-db bandwidth of a traveling-wave maser

$$B = B_m \sqrt{\frac{3}{G_{db} - 3}} . \tag{25}$$

This derivation of bandwidth assumes a Lorentzian line shape. The actual emission line shape of a maser material depends upon a number of factors, and, at the present state of the art, is best determined experimentally.

The bandwidth variation given by (25) is quite different from that predicted for the cavity maser and it is apparent that the gain-bandwidth product increases at high gain, rather than reaching a constant as in the case of the cavity maser (CM).

The bandwidth variation with gain has been plotted in Fig. 1 for a traveling-wave and a cavity maser. The cavity maser was assumed to have a magnetic Q equal to that of the TWM. For a typical case, we may take 0.05 per cent Cr^{+++} in Al_2O_3, for which B_m is 60 mc for operation at 6 kmc with the magnetic field at 90° to the crystal axis. In this operation, a magnetic Q of 150 is obtainable at 1.5°K. The gain of a cavity maser has been calculated, taking into account the effect of χ'

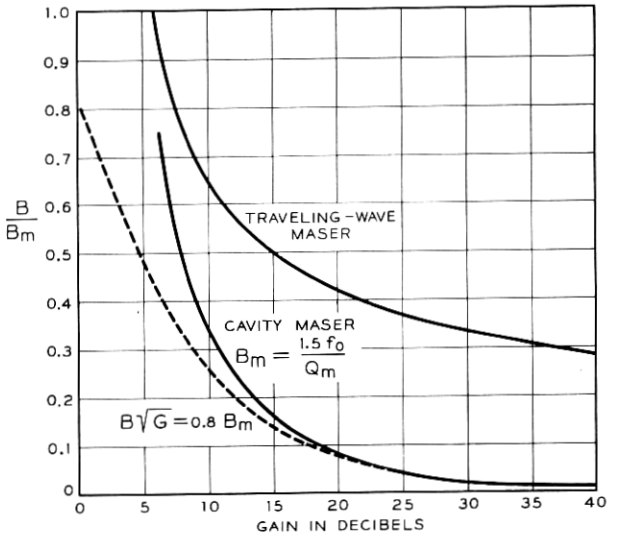

Fig. 1 — Normalized maser bandwidth, B/B_m, as a function of gain for the cavity maser and the traveling-wave maser.

from (24), as

$$G_{CM}^{1/2} = \frac{(1 - jb_0)(1 + jb_m) - R_0/R_m}{(1 + jb_0)(1 + jb_m) + R_0/R_m}, \tag{26}$$

where

$$b_0 = \left|\frac{R_0}{R_m}\right| \frac{2\Delta f}{f_0} Q_m, \tag{27}$$

$$b_m = 2\frac{\Delta f}{B_m}, \tag{28}$$

R_0 = the effective load impedance of the circulator,

R_m = the effective resistance of the maser material

and

Q_m = the magnetic Q of the maser material.

In the limit of large gain, the gain-bandwidth product approaches a constant given by (26) as

$$G_{CM}^{1/2} B = \frac{2}{\left(\frac{Q_m}{f_0} + \frac{1}{B_m}\right)}. \tag{29}$$

For the assumed maser operation in ruby,

$$G_{\mathrm{CM}}{}^{1/2}B = 0.8\ B_m\ . \tag{30}$$

The gain-bandwidth curve from (30) is plotted as a dashed line in Fig. 1. It is interesting to note that, for relatively low gains in the cavity maser, the true bandwidth given by (26) is somewhat greater than is estimated from the limiting gain-bandwidth figure of merit.

The required amplifier slowing and length can be determined from (22). Taking the above example for ruby operation at 6 kmc with Q_m equal to 150 and a structure length of 2 wavelengths (10 cm), we find that a slowing of about 90 is required in the slow-wave structure in order to give a gain of 30 db. An amplifier designed without geometric or resonant slowing, but using the dielectric constant of ruby, would require a length of about 300 cm. The TWM bandwidth for the assumed Lorentzian line shape would be 20 mc. A cavity maser designed using the same material would have a bandwidth of about 1.5 mc. It should also be pointed out that, since a broadband structure is used in the TWM, stagger tuning of the maser material along the maser structure can lead to even greater bandwidths.

The TWM has another important advantage over the cavity maser in that the useful slow-wave structure bandwidth may be an order of magnitude, or more, greater than the maser material bandwidth. Therefore, the center frequency of the maser passband can be tuned electronically over a wide frequency range simply by changing the pump frequency and the dc magnetic field. Thus, a TWM with a 20-mc passband may be tuned over a 200- to 500-mc frequency range at 6 kmc.

An important consideration in maser amplifiers is the sensitivity of the gain to a slight change in the material inversion as measured by χ''. We may, therefore, define the ratio of percentage change in gain to the percentage change in χ'' as a measure of this gain sensitivity, s_g. The gain sensitivity factors for a cavity maser and a traveling-wave maser are respectively,

$$\mathrm{CM}: s_g = \sqrt{G}, \tag{31}$$

$$\mathrm{TWM}: s_g = \log_e G. \tag{32}$$

These two equations are plotted in Fig. 2. They show that, at a gain of 30 db, the stability of a TWM is better by a factor of 4.6 than that of the cavity maser. Ultimately, gain stability in a maser is obtained by stabilization of the material χ'' through temperature regulation and regulation of the pump power. It is also advantageous to use sufficient pump power to saturate the pump transition and, hence, make χ'' rela-

tively insensitive to pump power. These techniques are applicable to both the cavity and the traveling-wave maser, but the stability factor, which is given by s_g, is always better in the TWM case. Gain stability may be an important factor in system applications as it has been in noise figure measurements, where the gain fluctuations are equivalent to actual system noise.

The gain stability to load changes of a TWM is also much better than that of a cavity maser. This problem is particularly bad in the case of the cavity maser, because of the dependence of the gain upon the iris coupling factor. This leads to gain changes due to thermal expansion and vibration effects.

The power output of a cavity maser, as well as that of a TWM, is limited by the total volume of active maser material present in the structure. In the case of the cavity maser, this volume is quite small, whereas a TWM uses a long interaction region and the volume of material is greater, often by an order of magnitude. As a result, in the case of the TWM a much wider dynamic range is to be expected, with output powers an order of magnitude greater. It is also possible to optimize output power by proper design of the slow-wave structure in order to increase active material volume.

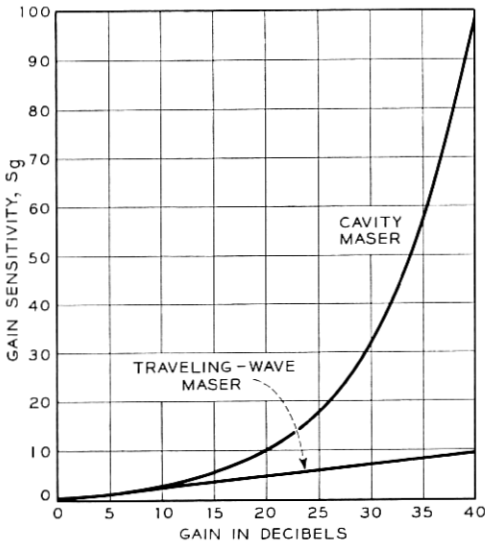

Fig. 2 — Pump saturation gain sensitivity, s_g, as a function of gain for the cavity maser and the traveling-wave maser.

Just as in the case of the cavity maser, some provision must be made in the propagating structure to allow either a propagating or cavity mode at the pump frequency in order to energize the emissive transition in the material. Finally, ease of fabrication and small size are necessary to the practical realization of the TWM.

III. SLOW-WAVE MASER STRUCTURES

There are three classes of structures suitable for slowing propagation for use with the TWM. The first class uses geometric slowing, such as one obtains in a helix where the energy is propagated on a long circuitous path. The second class uses resonant slowing, as is obtained in a periodic structure in which the energy is internally reflected in the various periods of the structure. The third class employs dielectric slowing and may be used in combination with either of the first two classes. The simple helix structure has an advantage in that it will produce high slowing over a very wide bandwidth of frequency, whereas periodic structures obtain slowing at the expense of tunable bandwidths. However, the circular polarization present on a helix structure has a plane which rotates around the axis of the helix. As a consequence, one requires a spiraling dc magnetic field in order to have the dc field perpendicular to the circularly polarized RF field.

The flattened helix structure of Fig. 3 is a possible broadband slow-wave structure which does have planar regions of circularly polarized magnetic field. The plane of circular polarization is perpendicular to the flat side of the helix and to the direction of propagation. Changes in the sense of polarization are indicated by the arrows.

The second class of slow-wave structures, the periodic type, has a definite passband with associated upper and lower cutoff frequencies.

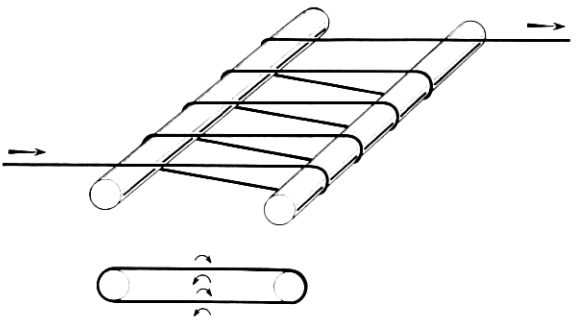

Fig. 3 — Flattened helix structure for broadband nonreciprocal gain.

In general, the narrower the structure passband, the higher is the slowing. It is quite possible to obtain slowing factors of 100 to 1000 in a periodic structure, while 10 to 100 is typical of a helix or other geometrically slowed structure.

It is interesting to note that, while many traveling-wave electron devices require constant phase velocity, the traveling-wave maser requires constant group velocity. As a result, various periodic structures which are very narrowband for tube applications, such as the comb structure, will have wide TWM bandwidths.

Also, it is essential to keep in mind that the structure must propagate at the desired pump frequency. This can be accomplished by propagating the pump power in a waveguide mode and locating the slow-wave structure in the waveguide in such a manner that the two structures are not coupled.

The TE_{10} mode in rectangular waveguide has an equipotential plane, as indicated by the cross section A-A in Fig. 4(a). Thus a planar arrangement of conductors in this cross section will have a minimum of coupling

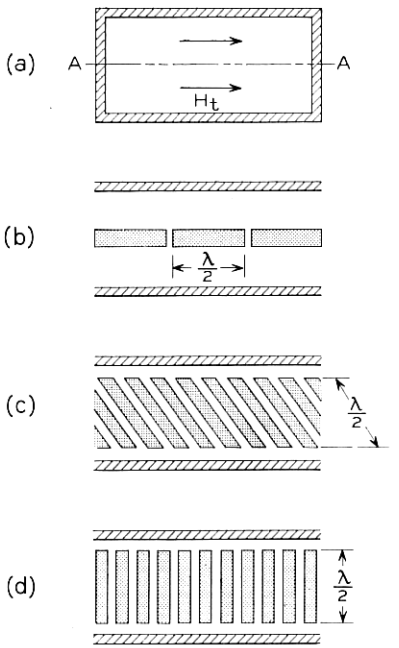

Fig. 4 — (a) The equipotential plane in TE_{10} waveguide and three parallel plane structures consisting of half-wave strip-line resonators: (b) end-coupled; (c) slant-coupled; (d) side-coupled.

to the waveguide mode. The flattened helix of Fig. 3 could be used in such a waveguide, although some coupling of the two modes would result. Three periodic-type structures consisting of coupled half-wave strip resonators are shown in Figs. 4(b), (c) and (d). The end-coupled arrangement of Fig. 4(b) is least desirable of these structures because the magnetic field is linearly polarized. The structure of Fig. 4(c), suggested by H. Seidel,[8] has mutual magnetic field coupling, which is variable by changing the slant angle. The structures of both Figs. 4(c) and 4(d) have regions of circular polarization of the magnetic field. The plane of circular polarization is perpendicular to the long dimension of the resonators of Fig. 4(d), and the sense of polarization is opposite above and below the plane of the strips.

Another set of slow-wave structures having planar conductors is shown in Fig. 5. Fig. 5(a) consists of an array of half-wave rods shorted to the side walls. Because of its symmetry, it can be shown that there is no component of Poynting's vector, $E \times H$, in the direction of the waveguide propagation. Consequently, it is a nonpropagating structure and has been suggested for use in the Easitron.[9] It is interesting because it points out the separate effects of electric and magnetic coupling between adjacent rods. A perturbation of the enclosing waveguide, such

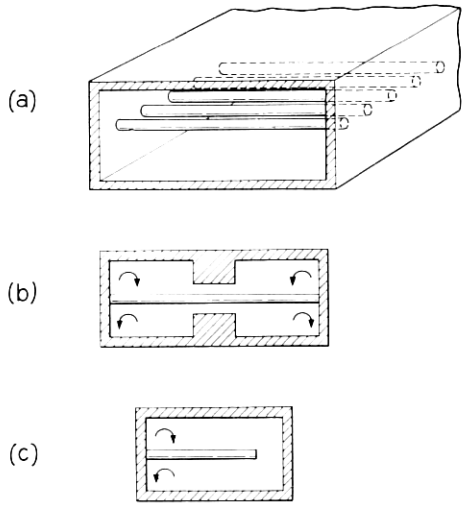

Fig. 5 — Structures consisting of planar arrays of conductors with electrical connection to the waveguide walls; the plane of circular polarization is perpendicular to the fingers and the arrows indicate changes in the sense of polarization: (a) Easitron zero passband structure; (b) Karp propagating structure; (c) comb propagating structure.

as that of the Karp[10] type of structure, in Fig. 5(b), produces a propagating passband in the structure. Thus, the Easitron structure may be called a zero passband structure in which the effect of electric and magnetic coupling between rods just cancels. The general properties of propagating parallel arrays has been discussed by Pierce.[11] Although the structure of Fig. 4(b) is similar to the Easitron, this structure will propagate, due to the fringe capacity at the ends of the resonators. The comb structure of Fig. 5(c) will have characteristics very similar to Fig. 4(d), since it is essentially Fig. 4(d) with a shorting plane along the center line, which is an equipotential plane for the slow-wave structure. A comb-type structure was used by Millman.[12] This structure had rather broad fingers, however, as required for effective electron beam interaction.

A rather extensive study of periodic slow-wave structures is given by Leblond and Mourier.[13, 14] A method for calculating the characteristics of such structures which takes into account coupling between nonadjacent wires was developed by Fletcher[15] and applied to the interdigital line. The interdigital line may be thought of as two comb structures attached to opposite walls of the waveguide with fingers interleaved. The interdigital line does not, in general, produce as much slowing as a comb structure, since, in its passband, the signal wave is propagated at the velocity of light along the circuitous path between adjacent fingers. Thus, the propagation does not depend upon a critical balance of finger to finger coupling and can take place without fringe capacity at the finger tips or a side-wall perturbation. A number of design curves for digital structures have been computed by Walling[16] using the theory of Fletcher. Nonreciprocal attenuation in the interdigital circuit has been analyzed and measured by Haas.[17]

IV. THE COMB-TYPE SLOW-WAVE STRUCTURE

As indicated by the arrows in Fig. 5(c), the comb-type slow-wave structure has regions of circularly polarized magnetic field above and below the plane of the fingers. Since the sense of polarization is reversed in the two regions, the structure is particularly suited to the TWM application.[18] The maser material can be placed on one side of the fingers and the isolator material on the opposite side. The magnetic field varies from a maximum at the shorted end of the rod to zero at the end. Since the electric field does just the opposite, it is possible to place a high dielectric material, such as ruby, in a region where effective magnetic interaction is obtained without incurring substantial dielectric loading, which might adversely effect the structure characteristics.

The microwave pump power is propagated through a waveguide enclosing the comb structure, such as in Fig. 6. The TE_{10} waveguide mode will produce strong longitudinal fields near the waveguide wall and transverse fields in the center of the guide. The dc magnetic field is applied in the direction of the fingers of the structure. Thus, for a maser crystal against the waveguide wall nearest the base of the fingers, $\Delta S = \pm 1$ pump transitions would be excited, while $\Delta S = 0$ pump transitions would be most strongly excited for a centrally located crystal. In our operation, both gadolinium ethyl sulfate and ruby maser materials have $\Delta S = 0$ pump transitions. Thus, it is necessary either to move the crystal away from the waveguide wall slightly, which reduces the gain, or to use a higher pump power, in order to invert the spin population throughout the crystal. The waveguide structure can, of course, be extended beyond the slow-wave structure. A waveguide short and coupling iris can then be used to obtain resonant enhancement of the pumping fields and, hence, better coupling to the pump transition in the crystal.

A perturbation measurement has been made, using a small sphere of ferrimagnetic material to measure the circularly polarized components of the magnetic field in such a comb structure. The absorption of the sphere at ferrimagnetic resonance is a measure of the circularly polarized filling factor per unit volume, which we will call F_+*. The result of such a measurement is plotted in Fig. 7. The dashed line in Fig. 7(b), labeled F_-*, is obtained either by reversing the direction of propagation through the structure or by reversing the dc magnetic field. The circularly polarized filling factor, F_+, and the figure of merit, R, can be obtained by integrating the appropriate curve over the cross section. This one

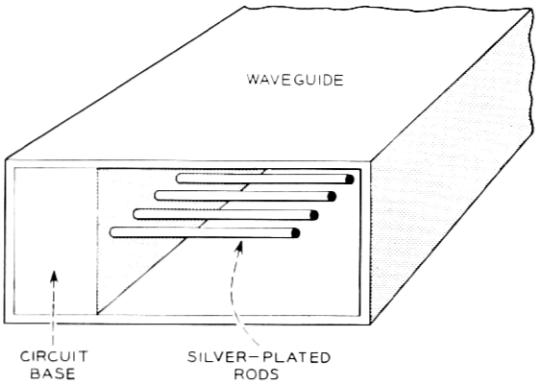

Fig. 6 — The comb-type slow-wave structure.

measurement is not sufficient to get the exact filling factor because the structure is not uniform. The filling factor should be calculated from measurements made over the volume of one period of the structure. The measurement of Fig. 7 predicts a forward-to-reverse gain ratio of about 15 for maser material between one side of the fingers and the wall. In actual tests on gadolinium ethyl sulfate, a value of R_m of 10 was obtained. Careful placement of ferrimagnetic sphere isolators in the same structure gave a value for R_i of 30.

The gain and tunable bandwidth of a maser using the comb structure can be computed from the phase-versus-frequency characteristics of the slow-wave structure. A useful equivalent circuit for this calculation is given in Fig. 8(a). The capacity, C_1, represents the fringe capacity at the ends of the fingers. The transmission line impedances, Z_{01} and Z_{02}, can be computed from the TEM characteristic impedance of the finger in waveguide transmission line at the upper and lower cutoff frequencies. When the phase shift between fingers is zero, the electric field pattern, Z_{++}, is that shown on the left in Fig. 8(b). The electric field pattern at

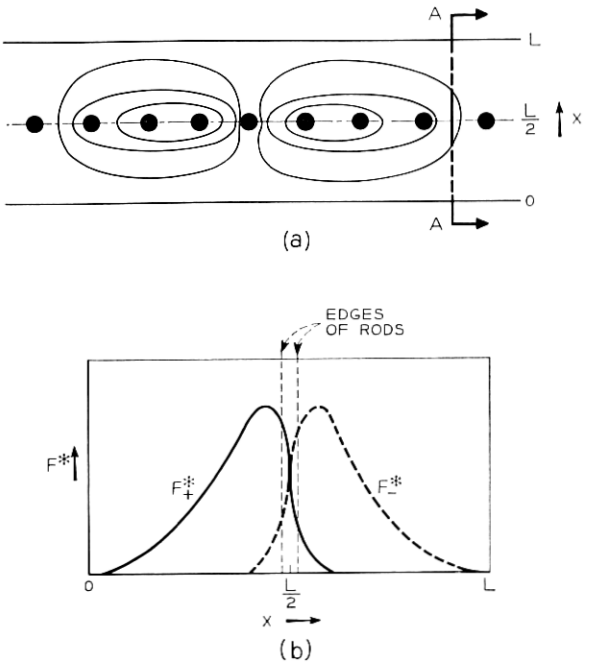

Fig. 7 — The magnetic field pattern (a) and measured amplitudes of circular polarized field components (b) for the comb-type slow-wave structure.

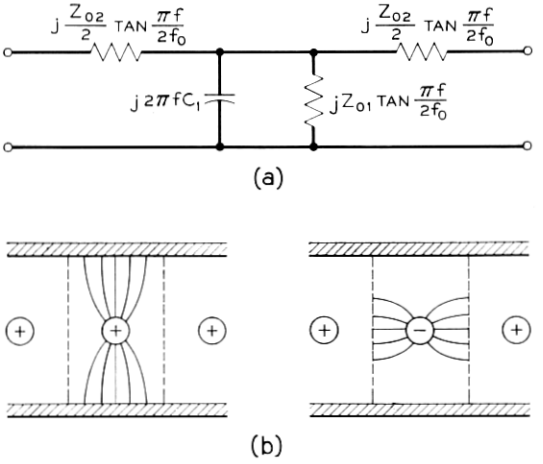

Fig. 8 — (a) Equivalent circuit for the comb structure and (b) the cutoff-frequency TEM mode electric field patterns.

the other cutoff frequency of the structure, Z_{+-}, is that corresponding to π phase shift, indicated on the right in Fig. 8(b). The impedances Z_{++} and Z_{+-} can be obtained analytically or by means of the usual electrolytic tank or resistance card analog computers. These cutoff impedances are related to those in the equivalent circuit by

$$Z_{01} = Z_{++}, \tag{33}$$

$$Z_{02} = \frac{4Z_{+-}}{1 - \frac{Z_{+-}}{Z_{++}}}. \tag{34}$$

The determinental equation for the circuit of Fig. 8(a) is

$$j2\pi f C_1 + \left(\frac{1}{Z_{01}} + \frac{2}{Z_{02}} \sin^2 \varphi/2\right) \tan \frac{\pi f}{2f_0} = 0, \tag{35}$$

where φ is the phase shift per section and f_0 is the frequency at which the circuit fingers have an electrical length of one-quarter wavelength. Solution of this transcendental equation is simplified by use of the curve in Fig. 9. The abscissa is the signal frequency normalized to f_0. The ordinate is $X_{co}Y(\varphi)$, which is given by

$$X_{co} = \frac{1}{2\pi f_0 C_1}, \tag{36}$$

$$Y(\varphi) = \frac{1}{Z_{01}} + \frac{4}{Z_{02}} \sin^2 \varphi/2. \tag{37}$$

The signal frequency for a certain phase shift is obtained by computing $X_{co}Y(\varphi)$, and then referring to Fig. 9.

The product SN required in the gain calculation can be obtained from experimental measurement of φ versus frequency from the equation

$$SN = N_s \frac{f_0}{2\pi} \frac{d\varphi}{df}, \tag{38}$$

where N_s is the total number of sections in the structure. For the equivalent circuit of Fig. 8(a), the SN product can be obtained from the curve of Fig. 10, which gives the quantity s, defined by

$$s \equiv \frac{SNX_{co}}{N_s Z_{02}} \sin \varphi. \tag{39}$$

Experimentally measured values of φ versus f were compared with the values calculated from the equivalent circuit, for a comb structure in which the end capacity, C_1, could be varied. The resulting calculations are shown in Fig. 11.

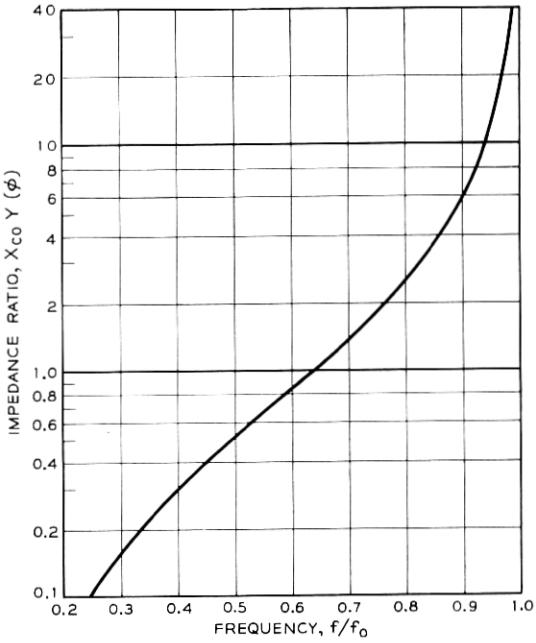

Fig. 9 — The curve, $X_{co}Y(\varphi)$ vs. f, used to solve equation (35).

The three curves were computed from the equivalent circuit analysis using the measured values of Z_{++} and Z_{+-}. The fringe capacity was determined by using the measured frequency for 0.2π phase shift. It should be mentioned that the equivalent circuit does not fully take into account the effect of coupling between nonadjacent fingers, an effect which may be important in this particular circuit.

A rather wide passband was obtained with the particular choice of parameters, even with rather large spacing between the finger ends and the opposite waveguide wall. Also, because of the wide bandwidth, the slowing varies over a wide range. The increase in slowing at the high-frequency end of the band is partially compensated for by the reduction

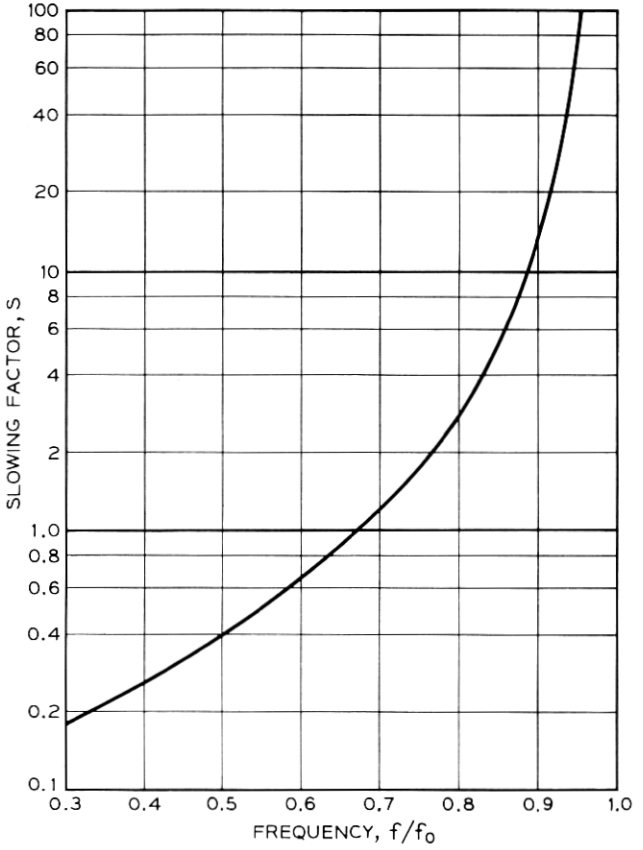

Fig. 10 — The slowing factor, s, as a function of frequency, used to determine SN from (39).

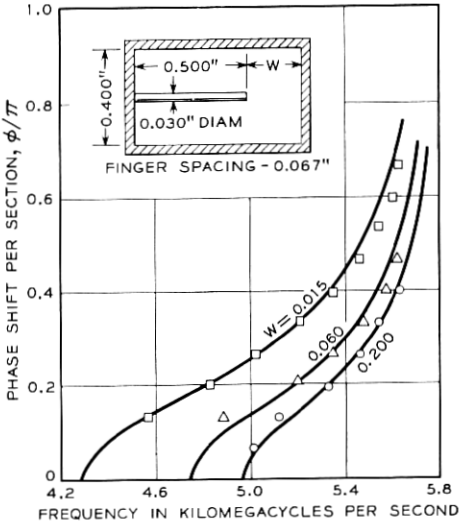

Fig. 11 — Phase shift per section, φ, vs. frequency, showing the effect of end wall capacity upon slowing.

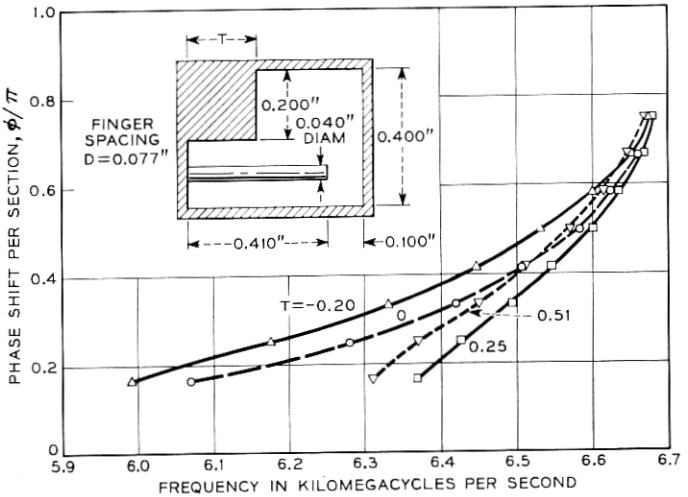

Fig. 12 — Phase shift per section, φ, vs. frequency showing the effect of a side wall perturbation upon slowing.

in the filling factor due to an increase in the stored energy between the fingers.

The structure passband can be decreased by reducing the waveguide height and increasing the distance between fingers. Too great a reduction in waveguide height will make the comb fingers a rather serious perturbation of the waveguide pump mode and will degrade the maser gain nonreciprocity factor, R_m. On the other hand, increasing the distance between fingers increases the over-all length of the amplifier.

Several methods for reducing the bandwidth of the comb structure have been tried. The first consisted of building a structure in which a wall perturbation could be moved across the width of the structure. The cross section of this test structure is shown in Fig. 12, along with the measured results obtained. The curve for $T = -0.2$ inch is for the case where the sliding side wall perturbation is pulled back from the base of the fingers. In this case, the bandwidth is increased. However, with $T = 0.25$ the bandwidth is reduced by a factor of 2 and relatively constant slowing is obtained over the band.

A second method for reducing the bandwidth is that shown in Fig. 13. The tips of the structure fingers are dielectrically loaded with a polystyrene strip having holes for the fingers. The dielectric increases the finger-to-finger capacity without greatly increasing the finger-to-wall capacity. Thus, this capacity would be in shunt with Z_{02} in the equivalent circuit of Fig. 8. It is apparent from the results in Fig. 13 that very narrow bandwidths can be obtained in this manner. However, the varia-

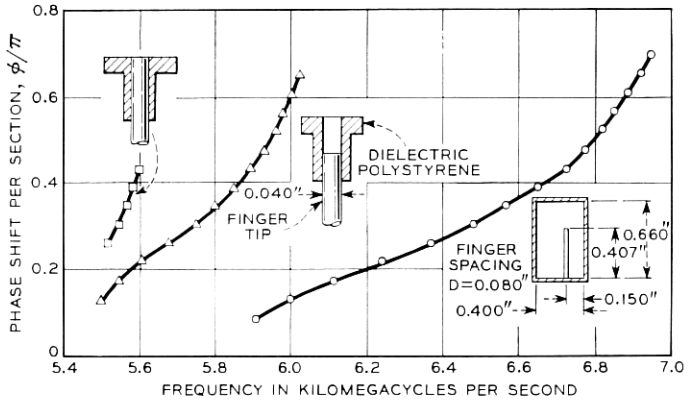

Fig. 13 — Phase shift per section, φ, vs. frequency, showing the effect of finger-to-finger capacity upon the slowing.

tions in structure dimensions become rather critical. Thus only a few points on the φ-f curve could be obtained using the structure resonance. This was also due in part to the high losses resulting from the high slowing.

The full-length ruby maser employed a slow-wave structure whose ρ-f characteristics are shown in Fig. 14. Notice that the unloaded structure has a wider passband than the final amplifier with dielectric loading of the ruby on both sides of the structure. In this case, the slowing was improved by not loading the ruby to the full height of each side of the waveguide. Thus, in this case, bandwidth narrowing is obtained by selective location of the maser material itself.

A number of different coupling schemes have been employed to match a 50-ohm coaxial cable into the comb structure. The matching arrangement shown in Fig. 15 gives quite broadband results. It has been found that a good impedance match can be obtained only over that frequency range for which the slowing factor is relatively constant. A VSWR less than 1.5 is typical over the useful band of the structure. Rapid variation of measured VSWR is observed which can be attributed to periodic variations in the structure which result in internal resonances. In actual maser operation, these internal resonances should be suppressed by the nonreciprocity of the structure.

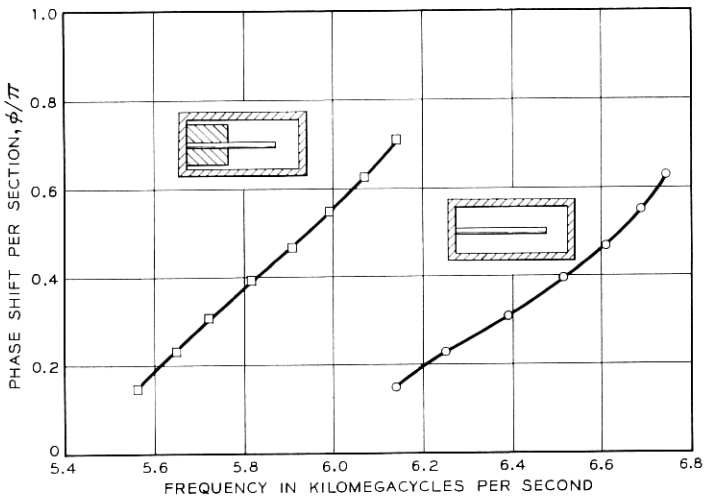

Fig. 14 — Phase shift per section, φ, vs. frequency for the comb structure used in the full-length ruby maser; the unloaded structure characteristic is compared with that of the ruby loaded structure.

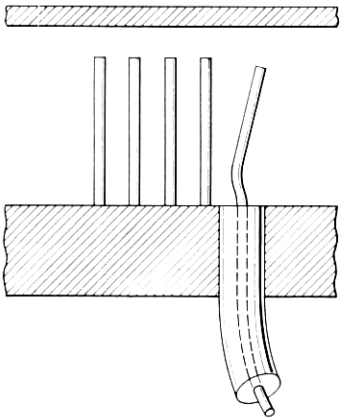

Fig. 15 — Detail of the coaxial-to-comb-structure impedance match.

V. GADOLINIUM MASER TEST SECTION RESULTS

The first TWM tests were performed using gadolinium ethyl sulfate as the active maser material and yttrium iron garnet as the isolator material. The cross section of this TWM is shown in Fig. 16. The slow-wave structure was similar to that of Fig. 12, since it employed a perturbation of the side wall to narrow the passband. Of course, the maser material dielectric constant also affected the structure characteristics and a certain optimum loading could be obtained.

Since the maser operation in gadolinium requires the pump magnetic field to be parallel to the applied magnetic field, a slab of dielectric was added against the waveguide wall to enhance the transverse RF waveguide magnetic field.

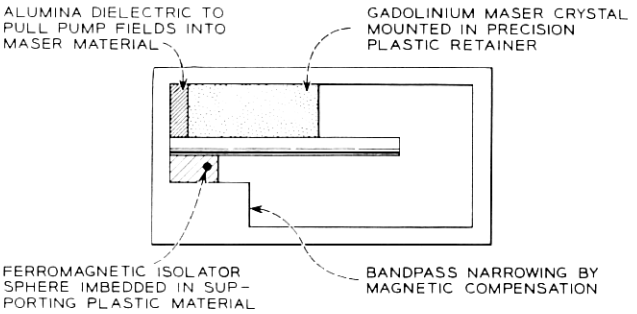

Fig. 16 — Cross section of gadolinium maser, showing location of active material and polycrystalline yttrium iron garnet isolators.

The "impurity dope" maser action in cerium-doped gadolinium ethyl sulfate produced at 1.6°K a magnetic Q_m of 170 in the structure used. The signal frequency was 6.0 to 6.3 kmc, and the pump frequency was 11.7 to 12.3 kmc. The magnetic field was about 1800 gauss. The nonreciprocity factor, R_m, was measured as about 10. The maser gain obtained was 12 db with about 1 inch of the slow-wave structure filled with the gadolinium salt. The active material consisted of three separate crystals which had to be accurately cut and aligned. Thus, it became apparent that the physical properties of the gadolinium salt were not too well suited for more than laboratory tests. The gadolinium bandwidth, B_m, was 30 mc.

It should be mentioned, however, that the maser operation in gadolinium does have the advantage of high saturation power and fast saturation recovery time. A power output of +15 dbm was obtained and the saturation recovery time was measured as about 20 microseconds.

The magnetic field required by the maser material is in the vicinity of that for ferrimagnetic resonance in a sphere. Hence, it was possible to use spheres of a gallium-substituted yttrium iron garnet, which was found to have a relatively high χ'' at liquid helium temperature. Spheres of yttrium iron garnet were located in the A-A cross section indicated in Fig. 7(a). By careful location of the spheres, approximately one per finger, an isolation ratio of 50 was obtained at room temperature. The isolation ratio at 1.5°K was 30.

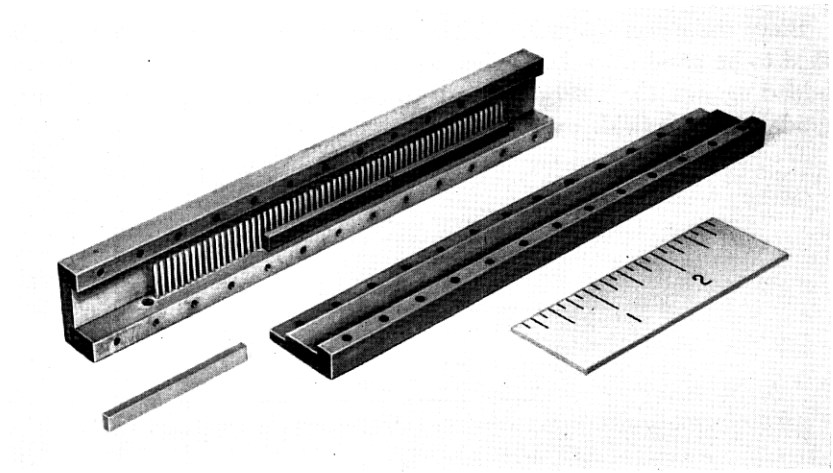

Fig. 17 — View of the disassembled comb structure for the ruby maser, with two pieces of ruby material shown in position.

VI. RUBY TRAVELING-WAVE MASER PERFORMANCE

The first high-gain full-length TWM was constructed using pink ruby which had approximately 0.05 per cent Cr^{+++} in the Al_2O_3 parent crystal. The slow-wave structure is shown in Fig. 17 with one side of the waveguide removed. Two pieces of ruby are shown in position, and a third is in the foreground. The comb structure has a length of 5 inches and consists of 62 brass rods approximately 0.4 inch long. The phase-shift characteristics of this structure were given in Fig. 14.

The holes for insertion of the coaxial input and output matches are visible at the ends of comb structure of Fig. 17. Fig. 18 is a cutaway drawing of the complete TWM assembly, showing the waveguide flanges which are added to the ends of the structure for attachment of a movable short and the pump waveguide coupling iris. This drawing also shows the location of the 0.05 per cent ruby amplifying material and the 1 per cent ruby isolator material. Notice that the 1 per cent ruby is spaced away from the circuit fingers by an alumina slab. This reduces the

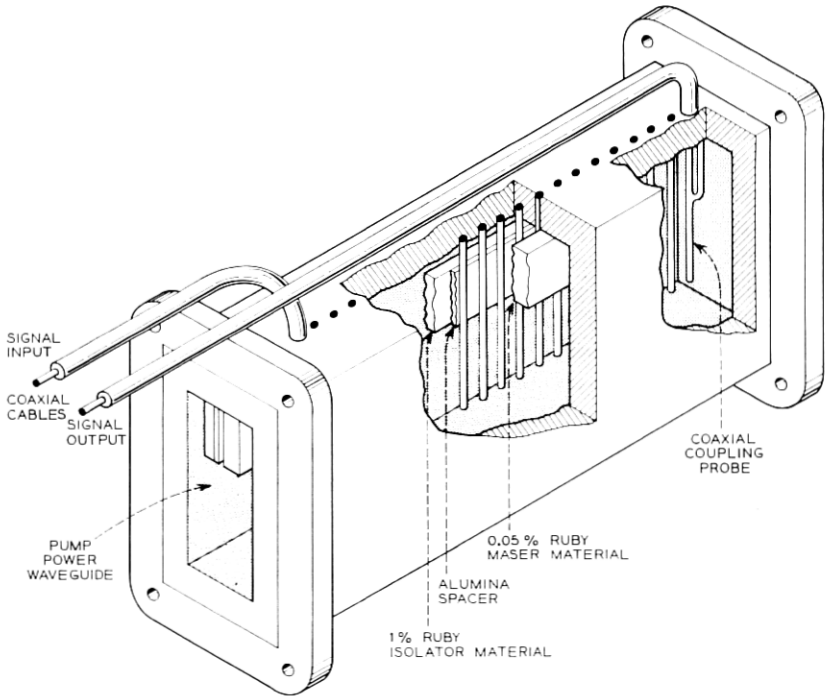

Fig. 18 — Cutaway view of full-length ruby maser assembly.

coupling of the isolator to the forward propagating circuit wave, thus improving the isolation ratio, R_i.

This TWM gives a net forward gain of 23 db and a net reverse loss of 29 db, including the input and output coaxial cables extending into the 1.5°K helium bath. With the dc magnetic field off, the structure gave a loss, L_0, of 3 db. The electronic gain of the maser material, the first term in (19), was 30 db, and the loss of the isolator was 35 db. Thus, the ratios R_m and R_i are about 3.5 and 8.5 respectively. The improved figure of merit for the isolator is due to the addition of the alumina slab. The high loss of the isolator, in spite of the spacer, is due to the increased Cr concentration.

The 3-db bandwidth of the TWM was measured as 25 mc at a center frequency of 5.8 kmc. This bandwidth is somewhat in excess of that predicted by an assumption of Lorentzian line shape as used in Fig. 1. The passband of the structure allows amplification over a frequency range of 5.75 to 6.1 kmc. The pump frequency must be tuned from 18.9 to 19.5 kmc and the dc magnetic field varied from 3.93 to 4.07 kilogauss to cover this electronic tuning range.

At a power output of -22 dbm, the gain of the amplifier is reduced by 0.5 db. The recovery time of the amplifier after saturation by a large signal is quite long, being on the order of 10^{-1} sec. This is due to the long relaxation time in ruby. It has one compensation, however, in that spin storage is very effective for increasing the pulse saturation power. Thus, with a pulse length of 10 microseconds and a pulse repetition rate of 100 per second, a pulse power output of $+8$ dbm was measured for the same 0.5-db reduction in gain. The saturation characteristic of a TWM is not abrupt, but is a smooth curve going to lower gain as the power is increased. In the limit of very high power, the TWM is essentially transparent. It will have an insertion loss of about 3 db, since after the maser material saturates, it produces neither gain nor loss.

The pump source had a power output of 100 mw. Recent experiments have been performed which show that satisfactory operation of the ruby TWM can be obtained with no waveguide iris and a short at the end of the amplifier. In this type of operation the pump power absorbed by the amplifier was less than 10 mw. The pump power absorbed by the amplifier determines the refrigeration power input required in a continuously cooled system. Thus a factor-of-10 reduction in maser pump power has a substantial effect upon the size of refrigerator required.

As was mentioned previously, it should be possible to obtain greater bandwidths in a TWM by stagger-tuning of the maser material. This was verified in this amplifier by rotating the maser magnet, which re-

sulted in tuning of the three maser crystals to different frequencies. A bandwidth of 67 mc at a gain of 13 db was measured.

VII. TWM NOISE-TEMPERATURE MEASUREMENT

Because of the high gain stability inherent in the TWM it was possible to perform a quite accurate measurement of noise temperature. Also, since the TWM is a unilateral two-port amplifier by itself, no external isolators or circulators are required when it is used, for instance, as a radar preamplifier.

The experimental system for the noise-temperature measurement is shown in Fig. 19. Two noise sources, which are matched loads maintained at different temperatures, are connected alternatively to the TWM input with an electrically operated waveguide switch. Isolators were included at the input and output of the TWM. Although the TWM is short-circuit stable, small gain fluctuations can be produced by changes in the input VSWR. Since gain fluctuations on the order of 0.02 db are significant in this measurement, an input isolator was included to eliminate gain changes when the waveguide switch is operated. An isolator was included on the output of the TWM to insure that no excess noise from the traveling-wave tube (TWT) would be fed back into the TWM

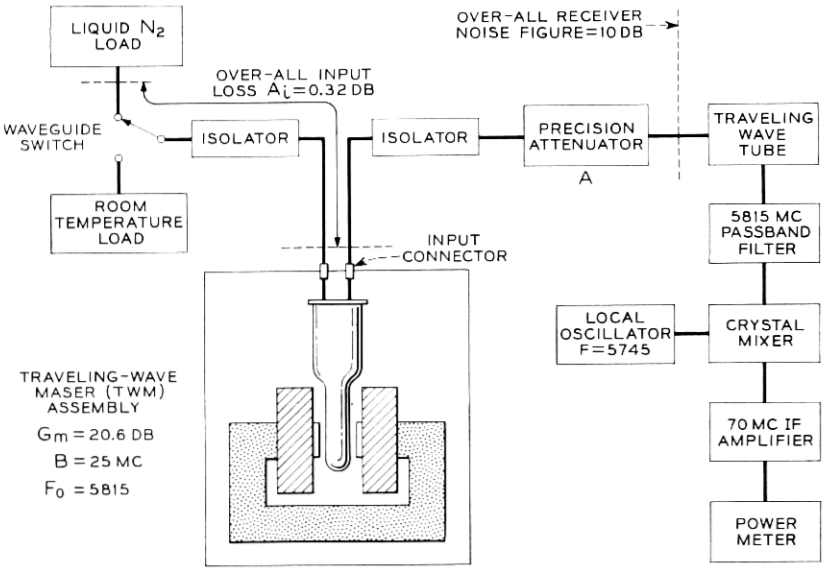

Fig. 19 — Experimental system for TWM noise temperature measurement.

and prevent maser gain changes because of the precision attenuator setting.

The microwave detecting system consisting of the TWT, filter, crystal mixer, etc., had an over-all noise figure of 10 db. The actual noise temperature measurement is made by switching the noise source and adjusting the precision attenuator to maintain constant output power at the power meter.

A total of 37 separate measurements were made over a period of about 30 minutes, and the resulting noise temperature was calculated to be

$$T_m = 10.7 \pm 2.3°\text{K}.$$

Approximately two-thirds of the estimated error was a statistical variation in the observed attenuator reading. About half of this attenuator reading variation can be attributed to gain fluctuations in the system of about ± 0.03 db during any one measurement and the other half to observational error. The remaining error is principally due to an error of ± 0.02 db in the determination of the input circuit loss, A_i.

Since the above-measured noise temperature is referred to an input connector at room temperature, it is a useful system temperature and the noise figure of the resulting preamplifier TWM is

$$F = 1.037 \pm 0.008 \ (0.16 \pm 0.03 \text{ db}).$$

The TWM employs half-inch diameter 50-ohm coaxial input and output leads of low heat conductivity monel to reduce heat loss from the liquid helium bath which was maintained at a temperature of 1.6°K. The coaxial cables were silver plated and polished to reduce microwave losses. The input cable, 30 inches long, had a room temperature loss of 0.28 ± 0.02 db. The actual input cable temperature gradient was monitored with 12 thermometers throughout its length. A calculation, using this data and taking into account the known variation of the resistivity of silver with temperature, shows that a noise temperature of 9 ± 1°K is produced by the input cable losses.

Another possible type of noise is that fed back into the TWM output from the isolator at room temperature. In the TWM, this produces a negligible contribution at the input because of the reverse isolation.

The noise contributed by the maser proper depends upon the spin temperature and the ratio of spin system gain to the circuit loss. A theoretical noise temperature of 2.4 ± 0.2°K is thus calculated from maser noise theory.[19,20,21]

The theoretically calculated over-all TWM noise temperature is then

$$T_m(\text{theory}) = 11.4 \pm 1.2°\text{K}.$$

Since it is apparent that most of the above noise is contributed by the input cable, a second experiment is planned which will exclude the input cable loss and allow a more direct measurement of the actual noise temperature of the maser amplifier proper.

VIII. FUTURE STUDIES

An extensive investigation of the ferrimagnetic properties of various ferrite and garnet materials at liquid helium temperatures is being carried out by F. W. Ostermayer of Bell Telephone Laboratories. A number of materials look promising for application as isolators in the ruby TWM. A ferrimagnetic isolator can be expected to have lower forward loss, higher reverse isolation, and low pump-power absorption.

Further reduction of the TWM tunable bandwidth will increase the gain. Thus it should be possible to obtain useful wideband gain at a somewhat higher bath temperature, such as 4.2°K.

It appears that, by using high pump-frequency-to-signal-frequency ratios, it will be possible to build low-frequency traveling-wave masers with about the same percentage tunable bandwidth as the present 6 kmc amplifier. Accordingly, a number of suitable circuits are being investigated.

IX. ACKNOWLEDGMENT

The initial slow-wave structure investigation for TWM application was begun by H. Seidel, whose assistance is gratefully acknowledged. We would also like to thank A. Pohly for technical assistance and G. Shimp for computation and plotting of curves.

REFERENCES

1. Bloembergen, N., Proposal for a New-Type Solid State Maser, Phys. Rev., **104,** October 1956, p. 324.
2. Scovil, H. E. D., Feher, G. and Seidel, H., Operation of a Solid State Maser, Phys. Rev., **105,** January 1957, p. 762.
3. Scovil, H. E. D., The Three-Level Solid State Maser, Trans. I.R.E., **MTT-6,** January 1958, p. 29.
4. McWhorter, A. L. and Meyer, J. W., Solid State Maser Amplifier, Phys. Rev., **109,** January 15, 1958, p. 312.
5. Makhov, G., Kikuchi, C., Lambe, J. and Terhune, R. W., Maser Action in Ruby, Phys. Rev., **109,** February 15, 1958, p. 1399.
6. Schulz-DuBois, E. O., Paramagnetic Spectra of Substituted Sapphires—Part I: Ruby, B.S.T.J., **38,** January 1959, p. 271.
7. Schulz-DuBois, E. O., Scovil, H. E. D. and DeGrasse, R. W., this issue, p. 335.
8. Seidel, H., private communication.
9. Walker, L. R., unpublished manuscript.

10. Karp, A., Traveling-Wave Tube Experiments at Millimeter Wavelengths with a New, Easily Built Space Harmonic Circuit, Proc. I.R.E., **43,** January 1955, p. 41.
11. Pierce, J. R., Propagation in Linear Arrays of Parallel Wires, Trans. I.R.E., **ED-2,** January 1955.
12. Millman, S., A Spatial Harmonic Amplifier for 6-mm Wavelength, Proc. I.R.E., **39,** September 1951, p. 1035.
13. Leblond and Mourier, Etude des Lignes a Barraux a Structure Périodique pour Tubes Electroniques U.H.F., Ann. de Radioélect. **9,** April 1954, p. 180.
14. Leblond and Mourier, Etude des Lignes a Barraux a Structure Périodique—Deuxieme Partie, Ann. de Radioélect., **9,** October 1954, p. 311.
15. Fletcher, R. C., A Broadband Interdigital Circuit for Use in Traveling-Wave-Type Amplifiers, Proc. I.R.E., **40,** August 1952, p. 951.
16. Walling, J. C., Interdigital and Other Slow-Wave Structures, J. Elect. and Cont., **3,** September 1957, p. 239.
17. Haas, L. K. S., Unilateral Attenuation in the Interdigital Circuit, WADC TR 57-239, Wright-Patterson Air Force Base, Ohio, May 1957.
18. DeGrasse, R. W., Slow-Wave Structures for Unilateral Solid State Maser Amplifiers, I.R.E., WESCON Conv. Record, August 1958.
19. Shimoda, K., Takahasi, H. and Townes, C. H., J. Phys. Soc. Japan, **12,** 1957, p. 686.
20. Pound, R. V., Ann. Phys., **1,** 1957, p. 24.
21. Strandberg, M. W. P., Inherent Noise of Quantum-Mechanical Amplifiers, Phys. Rev., **106,** May 15, 1957, p. 617.